

# Reactive Plasma-Sprayed Aluminum Nitride-Based Coating Thermal Conductivity

Mohammed Shahien, Motohiro Yamada, Masahiro Fukumoto, Kazumi Egota, and Kenji Okamoto

(Submitted March 23, 2015; in revised form September 7, 2015)

Recently, thick aluminum nitride/alumina (AlN/Al<sub>2</sub>O<sub>3</sub>) composite coatings were successfully fabricated through the reactive plasma spraying of fine Al<sub>2</sub>O<sub>3</sub>/AlN mixture in the N<sub>2</sub>/H<sub>2</sub> atmospheric plasma. The coatings consist of AlN, Al<sub>5</sub>O<sub>6</sub>N,  $\gamma$ -Al<sub>2</sub>O<sub>3</sub>, and  $\alpha$ -Al<sub>2</sub>O<sub>3</sub> phases. This study will evaluate the thermal conductivity of these complicated plasma-sprayed coatings and optimize the controlling aspects. Furthermore, the influence of the process parameters on the coatings thermal conductivity will be investigated. The fabricated coatings showed very low thermal conductivity (2.43 W/m K) compared to the AlN sintered compacts. It is attributed to the phase composition of the fabricated coatings, oxide content, and porosity. The presence of Al<sub>2</sub>O<sub>3</sub>, Al<sub>5</sub>O<sub>6</sub>N and the high coating porosity decreased its thermal conductivity. The presence of oxygen in the AlN lattice creates Al vacancies which lead to phonon scattering and therefore suppressed the thermal conductivity. The formation of  $\gamma$ -Al<sub>2</sub>O<sub>3</sub> phase in the coating leads to further decrease in its conductivity, due to its lower density compared to the  $\alpha$ -phase. Moreover, the high porosity of the coating strongly suppressed the conductivity. This is due to the complicated microstructure of plasma spray coatings (splats, porosity, and interfaces, particularly in case of reactive spray process), which obviously lowered the conductivity. Furthermore, the measured coating density was lower than the AlN value and suppressed the coating conductivity. In addition, the spraying parameter showed a varied effect on the coating phase composition, porosity, density, and therefore on its conductivity. Although the N<sub>2</sub> gas flow improved the nitride content, it suppressed the thermal conductivity gradually. It is attributed to the further increase in the porosity and further decrease in the density of the coatings with the N<sub>2</sub> gas. Furthermore, increasing the arc did not show a significant change on the coating thermal conductivity. On the other hand, the influence of spray parameters was optimized by investigating the effect of simple heat treatment (at 1100 °C) as a function of the arc current and N<sub>2</sub> gas flow. The heat treatment improved the coating thermal conductivity at the different spray parameters. Thus, after heat treatment, the coating porosity,  $\gamma$ -Al<sub>2</sub>O<sub>3</sub>, Al<sub>5</sub>O<sub>6</sub>N strongly decreased and therefore the conductivity improved. On the other hand, the N<sub>2</sub> gas flow and/or arc current did not show any difference on the conductivity after heat treatment. Therefore, using higher N<sub>2</sub> gas flow and higher arc current is economically useless. Finally, although the obtained conductivity of the coating was not so high (compared to the AlN value), the main factors that govern the conductivity of such complicated plasma-spraying composite coating was realized. Herein, in order to fabricate high thermal conductivity AlN plasma spray coating, adjusting the phase composition, oxide content, porosity, and microstructure (at low N<sub>2</sub> gas flow rate and low arc current) through the post-heat treatment is the key factor.

**Keywords** aluminum nitride, arc current, N<sub>2</sub> plasma gas, reactive plasma spray, thermal conductivity

This article is an invited paper selected from presentations at the 6th Asian Thermal Spray Conference (ATSC 2014) and has been expanded from the original presentation. ATSC 2014 was held in Hyderabad, India, November 24–26, 2014, and was organized by the International Advanced Research Centre for Powder Metallurgy and New Materials (ARCI) and the Asian Thermal Spray Society.

**Mohammed Shahien**, Toyohashi University of Technology, 1-1, Tempaku-cho, Toyohashi 441-8580, Japan and Advanced Materials Department, Central Metallurgical R&D Institute (CMRDI), Cairo, Egypt; **Motohiro Yamada** and **Masahiro Fukumoto**, Toyohashi University of Technology, 1-1, Tempaku-cho, Toyohashi 441-8580, Japan; and **Kazumi Egota** and **Kenji Okamoto**, Fuji Electric Co., Ltd., Hino, Japan. Contact e-mail: mo.shahien@yahoo.com.

## 1. Introduction

Among nitride ceramics, the superior properties of the aluminum Nitride (AlN) have attracted a great interest from the researchers. Aluminum nitride has a unique combination of electrical and mechanical properties: high thermal conductivity (up to 320 W/m K for pure single crystal and 180–220 W/m K hot pressed material), low thermal expansion coefficient, high electrical resistivity (10<sup>13</sup> Ω cm), a large band gap of 6.2 eV, good chemical/physical stability at fairly high applications, high hardness (Hv 1400), and high resistance of molten metals, wear and corrosion (Ref 1–5). Such unique properties make the AlN a promising candidate for several electrical and electronic applications: such as electronic substrates, semi-conductor packages, heat sinks, crucibles and vessels for handling corrosive chemicals and molten metals, parts of semi-conductor equipment, and reaction vessels of etching. Furthermore, the higher thermal conductivity of AlN

makes it a promising candidate to replace the widely used  $\text{Al}_2\text{O}_3$  substrate (Ref 5).

Besides the development of AlN sintered compacts, it is possible to improve a lot of characteristics due to formation of AlN coatings onto the material surface. In general, the AlN films are fabricated by chemical vapor deposition (CVD) and/or physical vapor deposition (PVD) techniques. Although, it was possible to fabricate high-quality AlN thin films by these techniques, it was difficult to get thick coatings (more than 100  $\mu\text{m}$ ). It is attributed to the relatively low deposition rate of CVD and PVD techniques (Ref 6). The thin AlN films are suitable for various electrical applications: piezoelectric transducers, surface acoustic wave sensors (SAW's) deposited on silicon wafers, microwave filter, and as thin film bulk acoustic resonator (FBAR) used in mobile phones. Moreover, the AlN thin films are supposed to be a good competitive in sensor, actuator, ultrasound applications, and for microelectromechanical systems (MEMS). On the other hand, it is difficult to apply the AlN thin films in the structural parts applications (e.g., as protective layers in the reaction vessels of CVD, PVD, or etching, insulating for heat sinks and power devices), which require thick coatings.

Thermal spray is a generic term for a group of commonly used processes for depositing thick metallic, non-metallic (ceramic or plastic), or any desired combination of coatings (Ref 7, 8). It is defined as the method of coating application through the deposition of molten or semi-molten (softened) particles propelling onto a substrate with high deposition rates (several  $\mu\text{m}/\text{min}$ ). The major advantage of thermal spraying is the wide variety of spray materials and techniques (Ref 8). However, the fabrication of nitride ceramic coatings such as AlN has been considered to be impossible. This is due to the thermal decomposition of the AlN particles during spraying without a stable melting phase. The solution to fabricate AlN thermal-sprayed coatings is using the reactivity of thermal plasma which is usually used to melt and accelerate the spray materials.

Reactive plasma spraying (RPS) has been considered as a promising technique for in situ formation of AlN thermal-sprayed coatings (Ref 9-18). The process is based on the reaction of molten particles (metallic or non-metallic materials) with the surrounding active species in the plasma such as atom, ion, or radicals. In our previous studies, it was possible to fabricate AlN-based coatings through RPS of aluminum (Al) (Ref 9-14) and  $\text{Al}_2\text{O}_3$  (Ref 15-17) powders in  $\text{N}_2/\text{H}_2$  plasma. During spray, the particles react with the surrounding active nitrogen plasma collide and rapidly solidify on the substrate. Due to the low melting point of Al (660  $^\circ\text{C}$ ), the particles coagulate and aggregate together, and it was difficult to achieve complete nitridation. The remaining metallic Al phase decreases the excellent insulation properties of the AlN coatings. On the other hand, using the  $\text{Al}_2\text{O}_3$  powders avoided the contamination of the metallic Al phase in the coatings.

Furthermore, fabrication of plasma spray AlN/ $\text{Al}_2\text{O}_3$  coatings is considered as a promising candidate for the

future power electronic and semi-conductor substrate applications. Thus, it requires high insulation properties with high performance (AlN,  $\text{Al}_2\text{O}_3$ ), high thermal conductivity (AlN), and large range application technology (plasma spray coating). To apply plasma-sprayed AlN/ $\text{Al}_2\text{O}_3$  coatings in these applications, fabrication of thick coatings, increasing the AlN content, and evaluating the thermal conductivity of the coatings are required.

Recently, it was possible to fabricate thick AlN/ $\text{Al}_2\text{O}_3$  coatings with high nitride content through the RPS of fine  $\text{Al}_2\text{O}_3/\text{AlN}$  mixture (Ref 18). However, there is lack of information about the thermal conductivity of such complicated composite coatings (very high and very low thermal conductivity components) and generally it is difficult to predict its conductivity. Moreover, the task becomes more difficult and more challenging when dealing with reactive plasma-sprayed coating because of its complicated microstructure (it consists of splats, porosity, and interfaces).

Therefore, the target of this research is the evaluation of the thermal conductivity of the reactive plasma-sprayed AlN/ $\text{Al}_2\text{O}_3$  coatings and finding the main aspects and controlling factors. Furthermore, to optimize the fabrication process of AlN coating, the influence of some process parameters on the thermal conductivity will be investigated. The study will focus on finding, rationalization, and optimizing the factors that govern the conductivity of such complicated coating system.

## 2. Experimental Procedure

All spray experiments were carried out by an atmospheric plasma spray system (APS: 9 MB, Sulzer Metco, Switzerland) as illustrated in Fig. 1. The  $\text{N}_2$  and  $\text{H}_2$  were used as plasma gasses and the typical spray conditions are shown in Table 1. The flow rate of the  $\text{N}_2$  plasma gas varied from 100 to 160 SCFH (standard cubic feet per hour) with keeping its pressure at the standard conditions of 330.9 kPa. The  $\text{H}_2$  (2nd) plasma gas was kept at the standard flow rate conditions of 5 SCFH and pressure of 344.7 kPa. The spray distance was kept 150 mm from the gun exit.

The feedstock powder in this study is spray dried 60 wt.%  $\text{Al}_2\text{O}_3$  and 40 wt.% AlN mixture. Commercial fine  $\text{Al}_2\text{O}_3$  powder (1  $\mu\text{m}$ ; Kojundo Chemical Lab Co., Ltd., Saitama, Japan) was spray dried with commercial fine AlN powder (1.14  $\mu\text{m}$ ; Tokuyama Co., Tokyo, Japan) using L-8i spray dryer (Ohkawara Kakohki Co., Ltd., Yokohama, Japan). A 5 wt.% polyvinyl alcohol (PVA; Wako Pure Chemical Industries, Osaka, Japan) adhesive solution was used for mixture agglomeration. The details of the primary feedstock particle size, final mixture particle size distribution, and spray-drying parameters are shown in Table 2. The details of the spray-dried mixture, density, microstructure, and phase analysis, are shown in the previous study (Ref 18). The feedstock powder was supplied to the plasma jet with carrier gas of  $\text{N}_2$ .

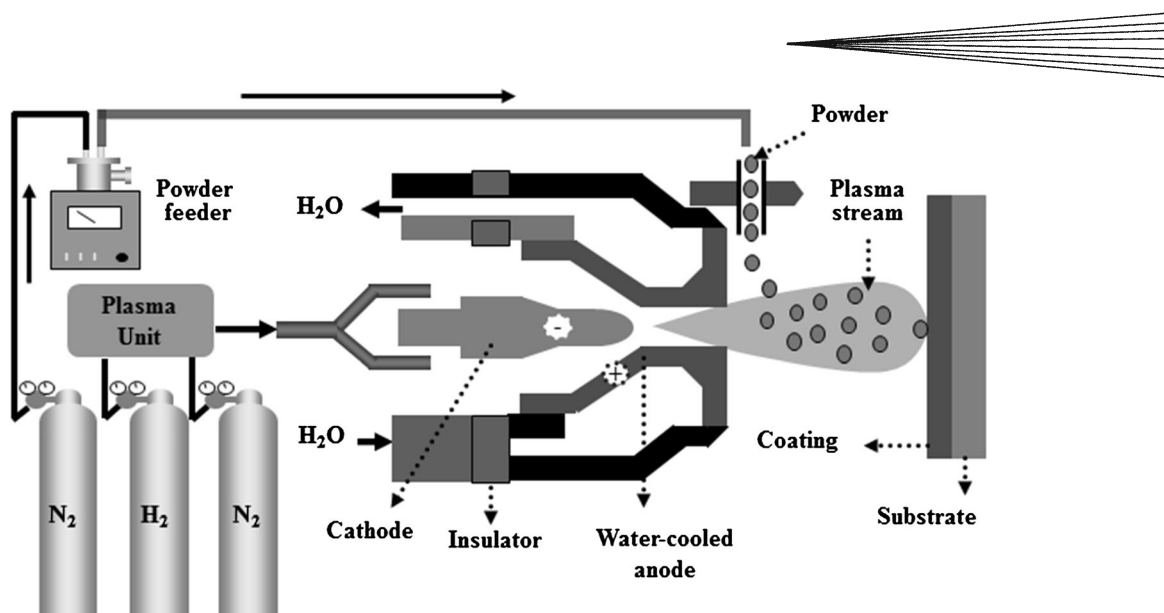


**Fig. 1** Schematic diagram of APS system

**Table 1** The typical spray conditions

1st gas: Pressure, kPa	N <sub>2</sub> : 330.9
1st gas: Flow rate, SCFH	N <sub>2</sub> : 100-160
2nd gas: Pressure, kPa	H <sub>2</sub> : 344.7
2nd gas: Flow rate, SCFH	H <sub>2</sub> : 5
Spray distance, mm	150
Arc current, A	500, 650
Carrier gas	N <sub>2</sub>

**Table 2** The feedstock powder details and spray-drying parameters

Primary feedstock powders particle size, $\mu\text{m}$	
AM	1.14
Al <sub>2</sub> O <sub>3</sub>	1
Spray-dried mixture particle size, $\mu\text{m}$	
D10	45.54
D50	54.68
D90	65.12
Spray dryer	L-Si
Disk type	MC-50
Rotational speed, rpm	20,000
Input temperature, K	473
Output temperature, K	378
Cyclone pressure, ( $\Delta P$ ) kPa	1
Solution color	White
Solution density	1.5
Solution viscosity, mPa s	960

The effect of post-treatment for the coating was investigated using an atmospheric furnace at 1100 °C for 6 or 12 h under N<sub>2</sub> gas flow. The post-heat treatment experiments were performed for the free standing coatings without substrate. The phase compositions of the fabricated coatings were verified by x-ray diffraction (XRD: RINT-2500, Rigaku, Tokyo, Japan) with Cu K $\alpha$  radiation. The scanning electron microscopes (SEM: JSM-6390, JEOL, Tokyo, Japan and SEM: S-4300, HITACHI, Japan)

**Table 3** The operating conditions for EPMA measurements

Accelerating voltage	15 kV
Irradiation current	30 nA
Measurement time	20 ms
Beam size	1 $\mu\text{m}$
Data point	250 $\times$ 190 point
Area size	1 $\times$ 0.76 mm
Analysis of x-ray and spectroscopic crystal	
C K $\alpha$ (44.6518 [Å])	LS12L
N K $\alpha$ (31.5909 [Å])	LS7A
O K $\alpha$ (23.5867 [Å])	LS5A
Al K $\alpha$ (8.3331 [Å])	RAP
Cu K $\alpha$ (1.5402 [Å])	LIF

were used to observe the cross-section microstructure of the coatings. The coating porosity was estimated by image analysis of the SEM cross sections. Furthermore, the Electron probe micro-analyzer (EPMA: EPMA-1610, Shimadzu electron beam micro-analyzer) was used for the elemental analysis, in order to investigate the nitriding content, composition ratio, and distribution of (N, O, Al, Cu, and C) in the fabricated coating cross section. The sample (disk-shaped coating) was re-polished and lapped after embedding resin to ensure the top and base of resin blocks are parallel. Prior the EPMA analysis, the embedded sample was coated with a thin film of carbon as conducting media to dissipate excess charge produced by the electron beam. Thus, the poor electrical conductivity causes serious charging problems, where shifting of the electron beam from the selected analysis position degrades spatial resolution or shifts the beam away from the selected analysis site. The system quantitatively analyzes the element distribution for elements with an atomic number greater than 5 (B: boron) to 92 (U: uranium) and the operating analytical conditions are shown in Table 3.

Thermal diffusivity and specific heat of the free standing coatings were measured at 25 °C by Laser Flash method and differential scanning calorimeter measurement, respectively. The samples were prepared in a disk shape with diameter of 10 mm and thickness about 0.5 mm. Thus, a disk-shaped masking was used in front of the pure copper (Cu) substrate to fabricate the free standing disk-shaped coatings. The samples front and back sides were polished in order to provide uniformity of the surface and to remove any Cu contamination from the substrate before measurement.

Thermal diffusivity of the samples was measured by the flash method using the LFA 447 Nanoflash<sup>®</sup> instrument (NETZSCH, Inc., Germany). Thus, the time that it takes for the heat to travel through the sample and causes

temperature increase on the rear face can be used to measure the through-plane diffusivity and calculate the through-plane thermal conductivity (if the specific heat and density are known) (Ref 19). Figure 2 simply shows the schematic of the through-plane measurement. The schematic diagram of the measurement process is sketched in Fig. 3.

The coating samples were coated with a graphite film before measurements, to give constant emissivity, to ensure complete and uniform absorption of the laser pulse and similar surface radiative characteristics in the sample. Furthermore, prior the diffusivity measurement, the coating samples were coated with Au (to avoid the penetration of laser pulse into the AlN and the errors in the measurement). The back side temperature increase was given following the JISR1611 and ISO18755 (Ref 20, 21) as follow:

$$\Delta T = \Delta T_m \left\{ 1 + 2 \sum_{n=1}^{\infty} (-1)^n \exp\left(-\frac{n^2 \pi^2 \alpha t}{L^2}\right) \right\}, \quad (\text{Eq 1})$$

where  $\Delta T [T(L,t)]$  is the instantaneous temperature increase of the back side (°C),  $\alpha$  the thermal diffusivity ( $\text{m}^2/\text{s}$ ),  $t$  the time (s),  $L$  the sample thickness ( $m$ ), and  $\Delta T_m$  is the maximum temperature increase of the back side (°C); it is given by the following equation:

$$T_m = \frac{Q}{\rho C_p L}, \quad (\text{Eq 2})$$

where  $Q$  is the quantity of input energy on the front face,  $\rho$  the density, and  $C_p$  is the specific heat.

By solving Eq 1, we get the backside temperature history curve. A typical temperature rise versus time is shown in Fig. 4. The thermal diffusivity had been deduced from Eq 1 and Fig. 4 by using the following expression:

$$\alpha = \frac{0.1388L^2}{t_{1/2}} * K, \quad (\text{Eq 3})$$

where  $t_{1/2}$  is the half maximum temperature increase (is the time required for the back side surface temperature to reach half of the maximum temperature rise: half of  $\Delta T_m$ ).

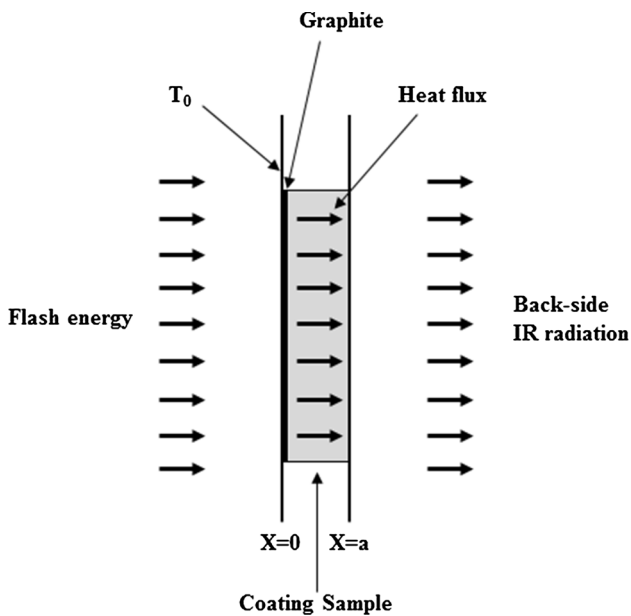


Fig. 2 Schematic diagram of the through-plane measurement method

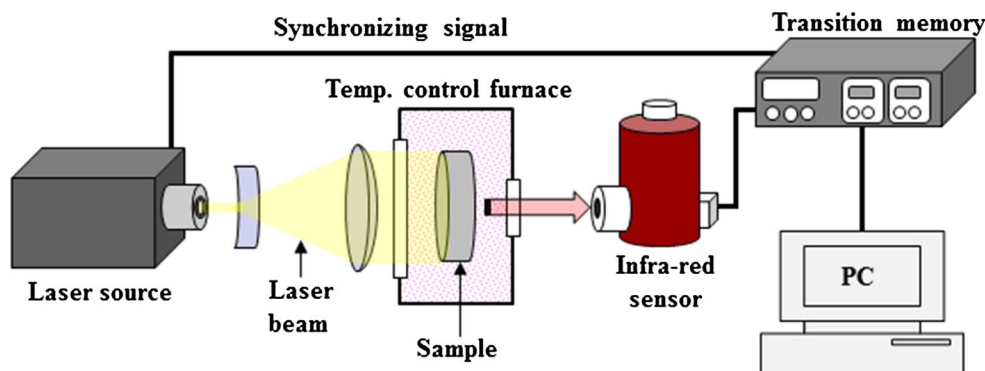


Fig. 3 Schematic diagram of the thermal conductivity measurement

The constant value of approximately 0.139 is known as the Fourier number.  $K$  is the energy loss constant and  $L$  is the sample thickness (m).

Therefore, the thermal diffusivity of the coating sample was calculated from its thickness ( $L$ ) and the time thermogram takes to reach half of the maximal temperature increase ( $t_{1/2}$ ). Equation 3 is a very useful expression for considering the optimum sample thickness.

The specific heat capacity (specific heat:  $C_p$ ) was measured using differential scanning calorimeter (Perkin-Elmer Co., DSC-7) comparative method, in the temperature range of 0-50 °C (measurement at 25 °C) with increasing rate of 10 °C/min in dry N<sub>2</sub> atmosphere. The specific heat of the material is defined as

$$C_p = \frac{Q}{m\Delta T}, \quad (\text{Eq 4})$$

where  $C_p$  is the specific heat (J/kg K),  $Q$  the quantity of required energy,  $m$  the mass, and  $\Delta T$  is the change in the temperature.

The principles of  $C_p$  measurement by using the DSC had been described before by O'Neill (Ref 22). The DSC measures the specific heat by heating the sample and comparing the sample temperature rise to the temperature rise of a reference sample (sapphire:  $\alpha\text{-Al}_2\text{O}_3$ ) of known specific heat tested under the same conditions as schematically shown in Fig. 5. The heat flow curves of the empty container (Perkin-Elmer standard Al case:  $\Phi$  6 mm  $\times$  1 mm), standard material (sapphire), and the coating crushed samples were obtained at the same measuring conditions. The temperature dependence of heat capacity was determined from these curves following the JIS R1672:2006 and JIS K7123:1987 (Ref 23, 24), by using the following equation:

$$\frac{D_{sa}(T)}{D_{st}(T)} = \frac{m_{sa}C_{p_{sa}}(T) + (W_{sa} - W_{bl})C_{p_{pan}}(T)}{m_{st}C_{p_{st}}(T) + (W_{st} - W_{bl})C_{p_{pan}}(T)}. \quad (\text{Eq 5})$$

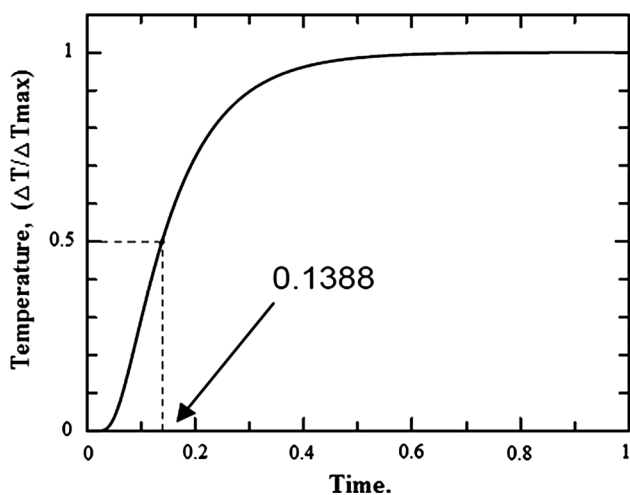


Fig. 4 Typical temperature rise on the back side of the sample in time function

By solving the equation, the sample specific heat capacity can be calculated as follow:

$$C_{p_{sa}}(T) = \frac{D_{sa}(T)}{D_{st}(T)} * \frac{m_{st}}{m_{sa}} * C_{p_{st}}(T) + \frac{D_{sa}(T)}{D_{st}(T)} * \frac{(W_{st} - W_{bl})}{m_{sa}} * C_{p_{pan}}(T) - \frac{(W_{sa} - W_{bl})}{m_{sa}} * C_{p_{pan}}(T), \quad (\text{Eq 6})$$

where  $D$  is the DSC (W),  $m$  the mass (kg),  $W$  the case weight (kg),  $C_p$  the specific heat (J/kg K), st the standard ( $\text{Al}_2\text{O}_3$ ), bl the blank, sa the sample (coating), and pan is the sample + case.

The sample bulk density was calculated from the measured sample volume (calculated from the measured sample dimensions) and mass by using the Shimadzu Co. electronic balance (AuW120D) at 25 °C. The measurement was done using the following equation:

$$\rho = \frac{m}{S * L}, \quad (\text{Eq 7})$$

where  $\rho$  is the density ( $\text{kg/m}^3$ ),  $m$  the mass (kg),  $S$  the surface area ( $\text{m}^2$ ), and  $L$  is the thickness (m).

Finally, the sample thermal conductivity can be calculated from the measured diffusivity, specific heat, and density as follow:

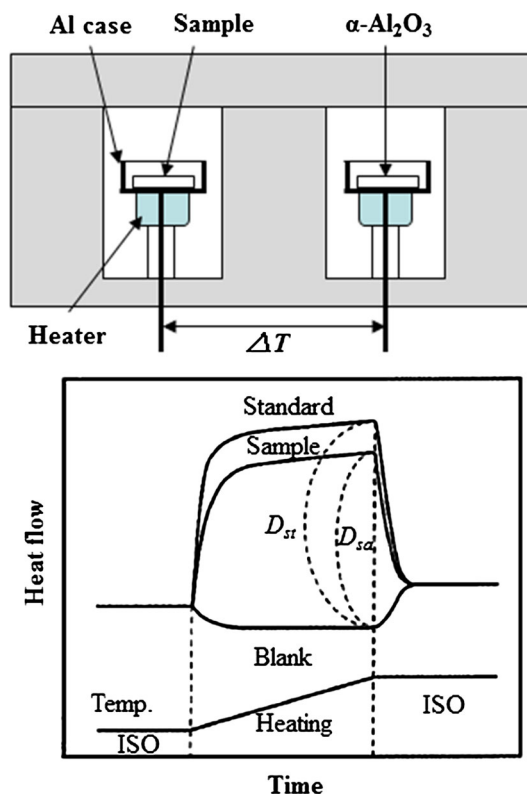


Fig. 5 Schematic diagram of the DSC measurement method

$$\lambda = \alpha \rho C_p, \quad (\text{Eq 8})$$

where  $\lambda$  is the thermal conductivity (W/m K),  $\alpha$  the thermal diffusivity ( $\text{m}^2/\text{s}$ ),  $\rho$  the density ( $\text{kg}/\text{m}^3$ ), and  $C_p$  is the specific heat ( $\text{J}/\text{kg K}$ ).

### 3. Results and Discussion

#### 3.1 As-Sprayed Coating Conductivity and $\text{N}_2$ Plasma Gas Effect

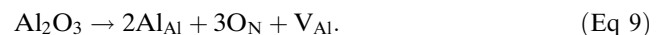
Table 4 shows the details values of the samples thickness and various components of the thermal conductivity values. The variation of the thermal conductivity and density of the fabricated coatings as function of  $\text{N}_2$  plasma gas flow rate has been plotted in Fig. 6.

It is clear that the thermal conductivity of the coatings is very low (2.43 W/m K) compared to AlN sintered compacts. The data also revealed that the further increase in  $\text{N}_2$  gas flow rate lowered the coatings thermal conductivity. The low thermal conductivity of the fabricated AlN coatings is mainly attributed to several factors: coating phase composition, oxide content, density, and porosity.

**3.1.1 The Effect of Phase Composition and Oxide Content.** The fabricated coating consists of cubic-AlN (*c*-AlN), hexagonal-AlN (*h*-AlN), aluminum oxynitride ( $\text{Al}_5\text{O}_6\text{N}$ ),  $\gamma$ - $\text{Al}_2\text{O}_3$ , and small content of  $\alpha$ - $\text{Al}_2\text{O}_3$  phases as shown in details in our previous study (Ref 18). The presence of such large amount of alumina significantly

lowered the thermal conductivity due to its low conductivity (10-30 W/mK for sintered samples) (Ref 5). Furthermore, formation of relatively large amount of oxynitride phase in the  $\text{Al}_2\text{O}_3$ -AlN system leads to further decrease in the fabricated coating thermal conductivity. This is due to the low thermal conductivity of oxynitride phase compared to the  $\text{Al}_2\text{O}_3$  itself (10 W/mK, Ref 25).

The presence of oxygen is the principle impurity in AlN industry, and it may lead to phonon scattering and therefore decrease in thermal conductivity of the polycrystalline AlN. The phase diagram between AlN and  $\text{Al}_2\text{O}_3$  shows the existence of oxynitride structure. Moreover, the AlN powders invariably contain some oxygen as typical contaminant located at the surface of the grains as alumina or oxynitride which spontaneously forms when AlN powder is exposed to air. Besides that, some oxygen is present in the AlN lattice in a dissolved form. The oxygen that has been dissolved in AlN lattice is essentially present as  $\text{Al}_2\text{O}_3$  dissolved in the lattice (Ref 26, 27). This oxygen (or  $\text{Al}_2\text{O}_3$ ) incorporation into the AlN lattice occupies nitrogen sites and creates aluminum vacancies to balance the electric charge as follow (Ref 26, 27):



Thus, the  $\text{V}_{\text{Al}}$  represents the Al vacancies. Such vacant aluminum sites lead to mass and strain misfits and this leads to increasing the scattering cross section of phonons, which decreases the phonon mean free path, thereby lowering the thermal conductivity (Ref 28). Thus, the

**Table 4** The thermal conductivity measurement values

$\text{N}_2$ gas, SCFH	Thickness $10^{-2}$ m	Density, $\text{kg}/\text{m}^3$ (a)			$C_p$ , J/kg K(b)	Diffusivity $10^{-6}$ $\text{m}^2/\text{s}$ (c)			$\lambda$ , W/m K(d)
		$m$ , $10^{-3}$ kg	$S$ , $10^{-4}$ $\text{m}^2$	$\rho$		$T_{0.5}$ , $10^{-3}$ S	$K$	$\alpha$	
100	0.0530	0.1075	0.8727	$2324 \pm 5$	$777.3 \pm 1$	27.90	0.963	$1.35 \pm 0.05$	2.43
120	0.0471	0.0860	0.8313	$2196 \pm 5$	$773.8 \pm 1$	17.83	0.971	$1.68 \pm 0.05$	2.86
160	0.0567	0.0830	0.7994	$1831 \pm 5$	$773.7 \pm 1$	42.35	0.963	$1.01 \pm 0.05$	1.43

(a) The density measurement using Eq 7. (b) Two samples were measured (using Eq 6) and the average was considered. (c) The diffusivity measurement using Eq 3. (d) The conductivity measurement using Eq 8  
 $\pm$  The uncertainty value for each measurement

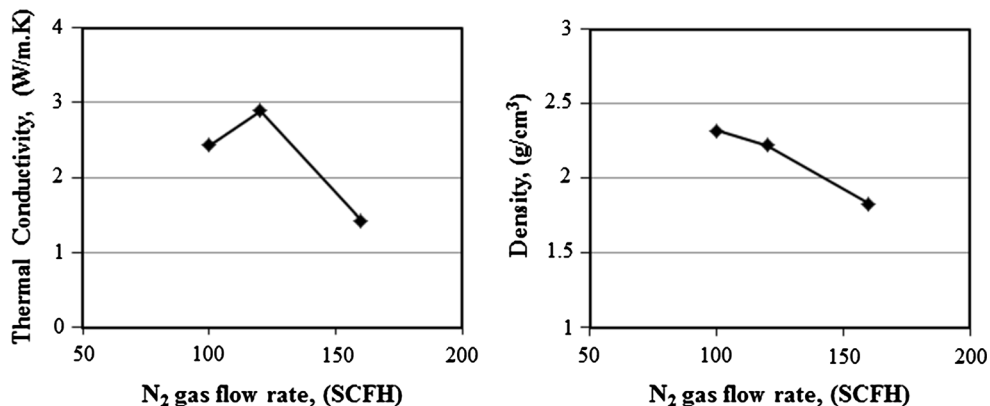


**Fig. 6** The thermal conductivity and density of the fabricated coatings vs. the nitrogen gas flow rate

oxygen has indirect role for decreasing the thermal conductivity. It indicates that theoretically if the aluminum oxide presents as  $\text{Al}_2\text{O}_2$  instead of the  $\text{Al}_2\text{O}_3$  form, no Al vacancies will appear and therefore the oxygen effect will decrease. Therefore, decreasing the dissolved oxygen is one of required factors to improve the thermal conductivity.

Furthermore, the high content of  $\gamma\text{-Al}_2\text{O}_3$  phase in the coating lowered the conductivity. As reported by Ault (Ref 29), the thermal conductivity of flame-sprayed  $\gamma\text{-Al}_2\text{O}_3$  coating is substantially less than the  $\alpha\text{-Al}_2\text{O}_3$  phase (it ranged from 0.050 W/cm K at 473 K to 0.027 at 1373 K). Thus, the  $\alpha\text{-Al}_2\text{O}_3$  phase is denser than the metastable  $\gamma\text{-Al}_2\text{O}_3$  phase. Furthermore, the low thermal diffusivity of  $\gamma\text{-Al}_2\text{O}_3$  phase is attributed to the relative disorder of the metastable phase as reported by Hurley and Gac (Ref 30). Thus, the decrease in the mean free path for the scattering of phonons was appropriate with large decrease in diffusivity. Moreover, the  $\gamma\text{-Al}_2\text{O}_3$  deposit has lower density ( $3.6 \text{ g/cm}^3$ ) than the  $\alpha$ -phase ( $3.98 \text{ g/cm}^3$ ) (Ref 29). Besides that, the  $\gamma\text{-Al}_2\text{O}_3$  has cubic spinel structure with higher Al(III) vacancies compared to  $\alpha\text{-Al}_2\text{O}_3$  (trigonal structure); all these factors decrease the  $\gamma\text{-Al}_2\text{O}_3$  thermal conductivity than the  $\alpha$ -phase.

The formation of  $\gamma\text{-Al}_2\text{O}_3$  in the coatings is related to the rapid quenching of molten  $\text{Al}_2\text{O}_3$  particles and the rapid solidification rate in the plasma spray process. Thus, the  $\alpha\text{-Al}_2\text{O}_3$  melted and the rapid quenching or solidification of the molten  $\text{Al}_2\text{O}_3$  spheres on cold surface leads to formation of  $\gamma\text{-Al}_2\text{O}_3$  crystals rather than  $\alpha\text{-Al}_2\text{O}_3$ . This transformation to the transient  $\gamma\text{-Al}_2\text{O}_3$  occurs easily under high temperature and rapid solidification rate of the plasma spray process, as we explained in details previously (Ref 18).

**3.1.2 The Effect of Coating Density, Porosity, and Microstructure.** The measured densities of the fabricated coatings are shown in Table 4 and Fig. 6. The coating density value ( $2.32 \text{ g/cm}^3$ ) is lower than the AlN value ( $3.16 \text{ g/cm}^3$ ) and gradually decreased with the  $\text{N}_2$  gas flow. Decreasing the coating density with the  $\text{N}_2$  gas flow rate can also clarify its extreme low thermal conductivity and the further decrease with the  $\text{N}_2$  gas flow rate.

On the other hand, Fig. 7 shows the front, backside photos, as well as the SEM cross-section microstructure of the fabricated coating at  $\text{N}_2$  gas flow of 100 SCFH. The coating is approximately  $500 \mu\text{m}$  thick with a uniform and porous structure. The presence of porosities scatter the phonons and the porosities are filled with air (it has poor conductivity), therefore the higher porosity, the lower the conductivity. Moreover, it is well known that the plasma-sprayed coating thermal conductivity is significantly lower than the corresponding bulk material (Ref 5, 31). It is attributed to the higher thermal resistance due to inter-lamellae boundaries (Ref 32) and porosity parallel to the coating plane (Ref 33). The plasma-sprayed coating consists of highly anisotropic layered structure with individual splats oriented parallel to the substrate surface, which lowered the thermal conductivity. It is related to the interfacial thermal contact caused by pores or secondary phases. Thus, the crystal lattice wave and heat wave are the main media through which heat is transported in ceramic materials, and dispersion as well as interference of the wave result from the coating pores lowers its conductivity. Moreover, in the RPS process, the porosity is higher than the normal plasma spray process due to the reaction between the particles and the surrounding active species in the plasma.

Additionally, it is worth to mention that the partial solidification and deposition mechanism of the splats in plasma spray process affect the coating conductivity. Thus, the residual stresses which occur during the cool down and the presence of un-melted particles between the splats lead to deficient bonding, cracks between splats. These imperfections lead to a thermal resistance which causes a large decrease in thermal conductivity. Therefore, the interfaces due to the thermal or impact stresses reduce the heat transfer by interface thermal resistance and therefore lower the thermal conductivity of the plasma spray coatings.

On the other hand, the further decrease in the coatings thermal conductivity with the increase in the  $\text{N}_2$  gas flow rate was clearly observed in Table 4 and Fig. 6. In order to clarify the  $\text{N}_2$  gas effect on the thermal conductivity, its effect on the phase composition, porosity, and density was

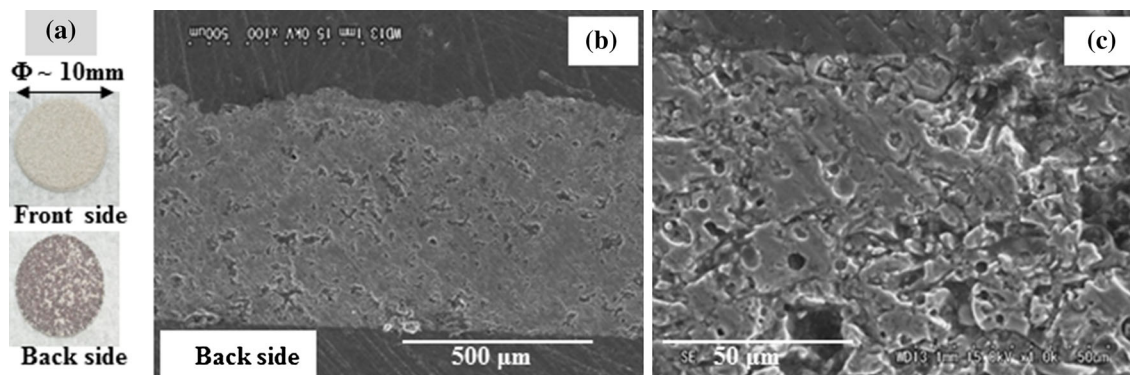


**Fig. 7** The fabricated coating at  $\text{N}_2$  gas flow of 100 SCFH: (a) sample front and backside photos, (b) SEM cross-section microstructure and (c) higher magnification of (b)

**Table 5** The N<sub>2</sub> gas flow effect on the coating density, porosity, and composition

Ni gas flow, SCFH	Density, g/cm <sup>3</sup>	Porosity, %	Phase content, %				
			<i>c</i> -AlN	<i>h</i> -AlN	γ-Al <sub>2</sub> O <sub>3</sub>	Al <sub>5</sub> O <sub>6</sub> N	α-Al <sub>2</sub> O <sub>3</sub>
100	2.32	15	17	27	31	24	3
120	2.22	17	8	34	29	23	6
160	1.83	26	2	42	26	19	11

considered. Table 5 summarizes the coating density, porosity, and phase content as function of N<sub>2</sub> gas flow rate. The coating density was calculated from the measured sample volume using Eq 7 as explained in the experimental part. The coating porosity was estimated by image analysis of SEM cross section. Moreover, the relative amounts of the assigned phases in the coatings were estimated by comparing the peak intensities from the XRD data using the following equation (Ref 34):

$$R_x = \frac{I_x}{I_{(113)}^{\alpha\text{-Al}_2\text{O}_3} + I_{(200)}^{c\text{-AlN}} + I_{(100)}^{h\text{-AlN}} + I_{(400)}^{\gamma\text{-Al}_2\text{O}_3} + I_{(311)}^{\text{Al}_5\text{O}_6\text{N}}}, \quad (\text{Eq 10})$$

where  $R_x$  is the concentration ratio and  $I_{(hkl)}$  is the intensity of the peak diffraction for the corresponding plane of *c*-AlN, *h*-AlN, α-Al<sub>2</sub>O<sub>3</sub>, Al<sub>5</sub>O<sub>6</sub>N, and γ-Al<sub>2</sub>O<sub>3</sub> phases.

It is clear that, although the N<sub>2</sub> gas flow improved the nitriding conversion (*h*-AlN content in the coatings), it increased α-Al<sub>2</sub>O<sub>3</sub> and decreased γ-Al<sub>2</sub>O<sub>3</sub> as well as Al<sub>5</sub>O<sub>6</sub>N (which are considered as positive effect to increase the thermal conductivity). The coating porosity gradually increased and the coatings density gradually decreased with increasing N<sub>2</sub> gas flow rate (which have negative effect on the coating thermal conductivity). Decreasing the coating density with the N<sub>2</sub> gas is strongly related to the significant increase in the porosity. Therefore, the thermal conductivity decreased with the further increase in N<sub>2</sub> gas flow rate. It is attributed to increasing the porosity and decreasing the density of the coating. Furthermore, it indicates that increasing AlN content did not show any significant effect to improve the conductivity of such complicated highly porous microstructure coating with high oxide content.

Increasing the porosity with the N<sub>2</sub> gas is related to increasing particle velocity with the N<sub>2</sub> gas. Thus, increasing the particle velocity shortened its residence time in the plasma and leads to worse melting behavior, which significantly affects the coating porosity. Furthermore, increasing the N<sub>2</sub> gas significantly lowers the plasma temperature and this suppresses the melting of the particle and therefore leads to higher porosity. Besides that, increasing the N<sub>2</sub> gas flow in the RPS process enhanced the reaction tendency between the particles and the surrounding plasma, which leads to increasing the coating porosity. This point is different from conventional plasma spray techniques, in which increasing the particle velocity and the driving force leads to a decrease of the porosity of

the coating. The effect of N<sub>2</sub> gas flow on the phase transformation of α-Al<sub>2</sub>O<sub>3</sub> to the γ-Al<sub>2</sub>O<sub>3</sub> phase is strongly attributed to the worse melting behavior of the particles with increasing the N<sub>2</sub> gas flow which leads to less phase transformation.

Due to the current low thermal conductivity values, the phase distribution and nitrogen distribution should be considered. Further, confirmation of the phase (N, O, Al, C, Cu) distribution and the Al, N, O ratio in the fabricated coating was done by the EPMA analysis. The EPMA concentration map and the Al, N, O line profile are shown in Fig. 8 and 9, respectively. It is clear that the Al, N, and O are homogeneously distributed in the coated sample. The Al, N, and O ratio in the coating, (including ZAF correction) are approximately estimated to be 1:4:4 roughly. In addition, the Cu had been unevenly distributed in the resin substrate side. Moreover, the voids are scattered in the coating. The composition contrast is almost uniform, and it is estimated that the resin has penetrated the voids.

Herein, the fabricated AlN coatings through RPS of Al<sub>2</sub>O<sub>3</sub>-AlN powder in N<sub>2</sub>/H<sub>2</sub> ambient had low thermal conductivity and lower density than AlN values. Furthermore, despite the significant effect of the N<sub>2</sub> gas flow rate on improving the nitriding conversion, it increased the coating porosity, lowered the density, and therefore lowered the thermal conductivity. It reveals that not only the AlN content and its distribution are the required points to get high thermal conductivity coatings but adjusting the oxide content and coating porosity is also required. To optimize the spraying parameters regarding the thermal conductivity, the next section will investigate the effect of arc current and simple heat treatment on the fabricated coatings and its thermal conductivity.

### 3.2 Spray Parameters Optimization Regarding Thermal Conductivity

In this section, the coatings were fabricated through changing the arc current and N<sub>2</sub> gas flow rate. Figure 10 shows the XRD spectra of the feedstock spray-dried powder, the coating fabricated with using N<sub>2</sub> gas of 100 SCFH at arc current 500 and 650 A, as well as the heat-treated coating (650 A). The feedstock powder consists of *h*-AlN and α-Al<sub>2</sub>O<sub>3</sub> phases, Fig. 10(a). After spraying at arc current 500, the fabricated coatings consist of *c*-AlN, *h*-AlN, Al<sub>5</sub>O<sub>6</sub>N, γ-Al<sub>2</sub>O<sub>3</sub>, and small amount of α-Al<sub>2</sub>O<sub>3</sub> phases as shown in Fig. 10(b). With increasing the arc, the coating composition slightly changed as shown in



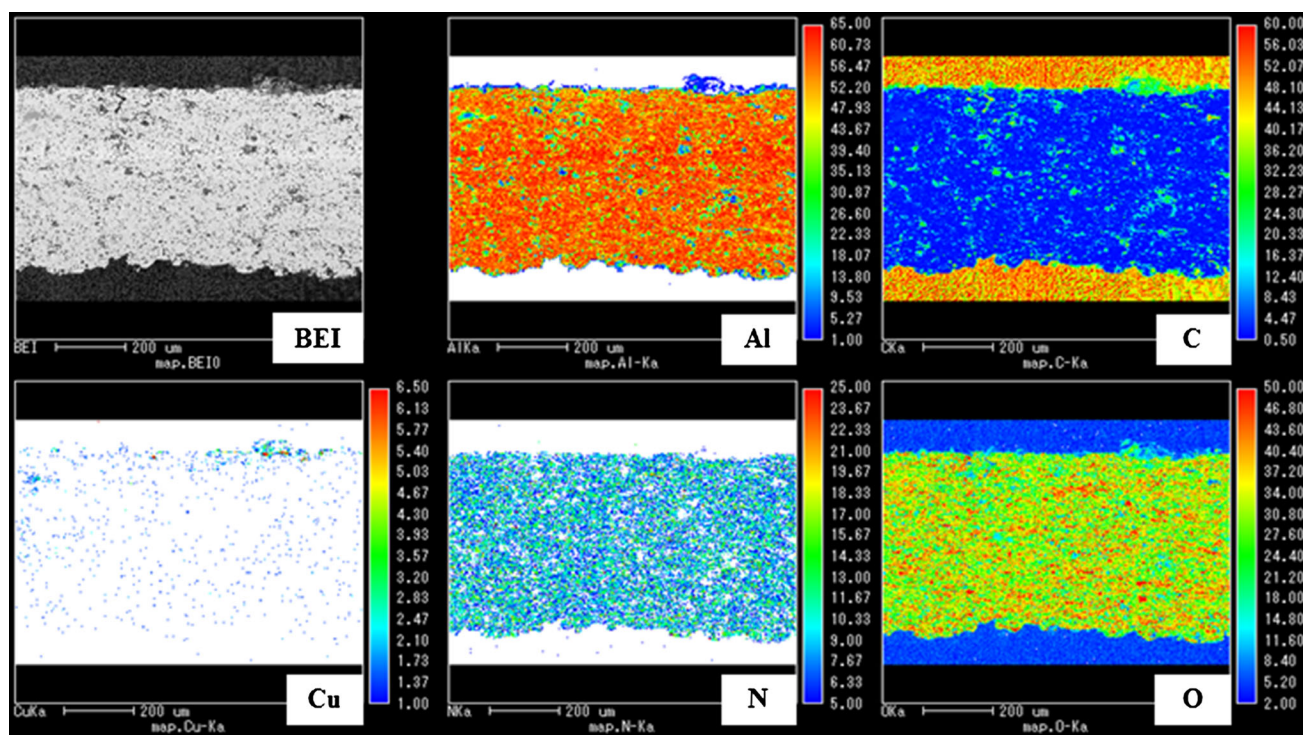


**Fig. 8** The EPMA map analysis of the cross section of the fabricated coating at  $N_2$  gas flow of 160 SCFH (Color figure online)

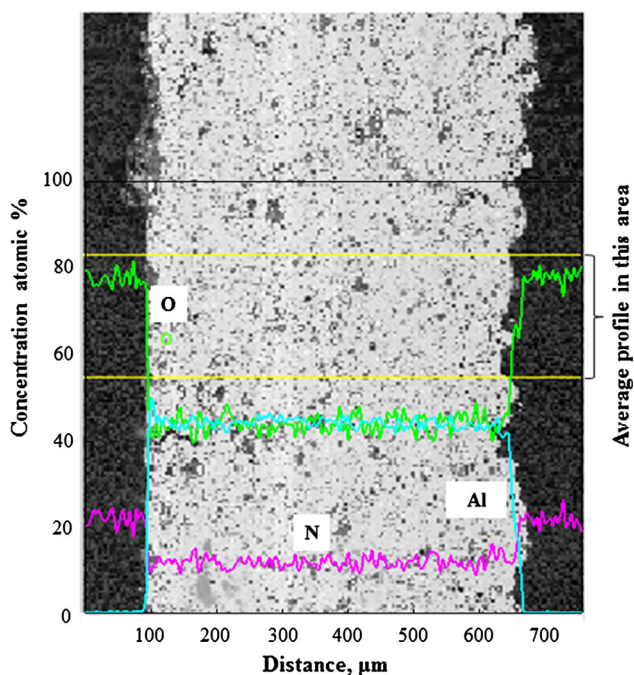


**Fig. 9** The line profile of the coating cross section fabricated at  $N_2$  gas flow of 160 SCFH

Fig. 10(c). The  $c$ -AlN content decreases and the  $h$ -AlN slightly improved. Furthermore, the complete transformation of the  $\alpha$ - $Al_2O_3$  to  $\gamma$ - $Al_2O_3$  phase was noticed after increasing the arc current. It is attributed to increasing the plasma temperature with the arc current. Increasing the temperature enhanced the transformation of  $c$ -AlN to the  $h$ -AlN phase as well as the melting of  $\alpha$ - $Al_2O_3$  particles and therefore assists its complete transformation, the  $\gamma$ - $Al_2O_3$  phase. On the other hand, after the heat treatment, the  $\gamma$ - $Al_2O_3$  phase transformed to the  $\alpha$ -phase (Fig. 10(d)), which is common in the plasma-sprayed  $Al_2O_3$  coatings at such conditions (Ref 35).

To optimize the spray parameters, the  $N_2$  plasma gas flow rate was increased to 160 SCFH at arc current 650 A. Figure 11 shows the XRD spectra of the coating fabricated with using  $N_2$  gas flow of 160 SCFH at arc current 650 A, as well as the heat-treated coating. It is clear that the as-sprayed coating composition changed after increasing the  $N_2$  gas with using higher arc current, Fig. 11(a). The  $h$ -AlN significantly improved,  $c$ -AlN content decreased, and  $\alpha$ - $Al_2O_3$  content increased compared to the coatings fabricated at the same arc current with lower  $N_2$  gas flow (Fig. 10(c): 650 A and 100 SCFH), and compared to the coatings fabricated at lower arc current and lower  $N_2$  flow and lower current (Fig. 10(b): 500 A and 100 SCFH).

It is attributed to the fact that the  $N_2$  gas flow rate improved the nitriding reaction due to the increasing of the nitriding species surrounding the particles and there-

fore facilitates the complete crystal growth to the *h*-AlN phase after deposition (through plasma irradiation) on the substrate, as explained in detail previously during RPS of Al<sub>2</sub>O<sub>3</sub> and Al<sub>2</sub>O<sub>3</sub>/AlN mixture (Ref 15, 18). The complete crystal growth of *c*-AlN to the *h*-AlN was significantly exhibited with using the fine particles compared with the large-size particles. Such observations are in a good agreement with Cao et al. reports (Ref 34), that the N<sub>2</sub> gas flow improves the nitriding conversion in the plasma spray process. Furthermore, it is also considered that, with increasing the N<sub>2</sub> gas flow, the plasma become colder and the particle become faster, and therefore, the decomposition of AlN feedstock will decrease and its content will increase in the deposited coatings. Therefore, increasing the N<sub>2</sub> gas flow rate improved the *h*-AlN content in the coating especially under such high temperature condition (with increasing the arc current).

On the other hand, increasing the N<sub>2</sub> gas flow rate suppressed the phase transformation of the fine  $\alpha$ -Al<sub>2</sub>O<sub>3</sub> feedstock particles during spraying to the  $\gamma$ -phase. Therefore, the  $\alpha$ -phase content slightly increased with the further N<sub>2</sub> flow rate. This is attributed to the colder plas-

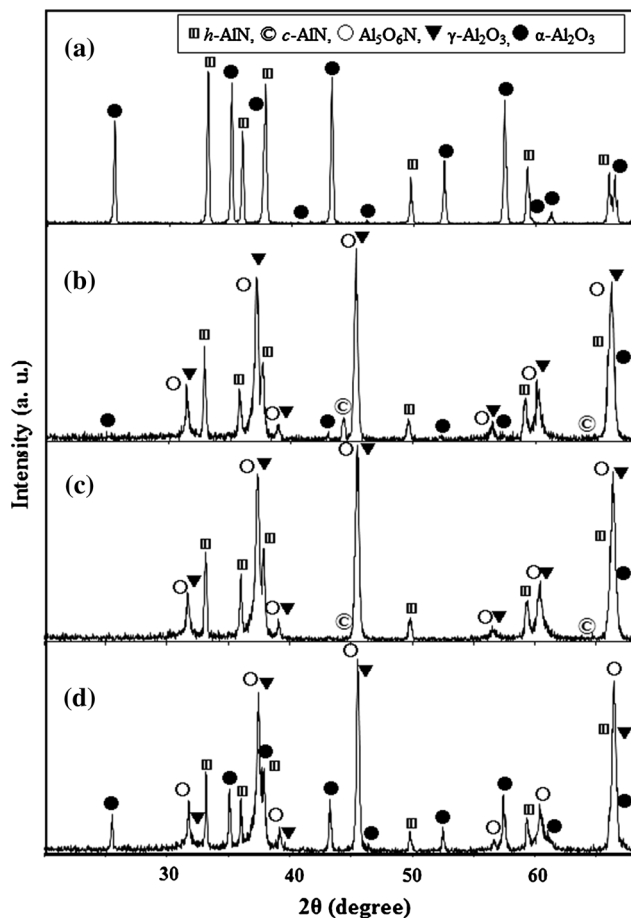


**Fig. 10** XRD spectra of (a) Al<sub>2</sub>O<sub>3</sub>/AlN spray-dried mixture and the fabricated coating with using N<sub>2</sub> plasma gas flow rate of 100 SCFH and using: (b) A.C. 500, (c) A.C. 650, and (d) A.C. 650 and heat treatment at 1100 °C for 6 h in N<sub>2</sub> gas ambient

ma, worse particle melting, and particles in-flight behavior or diagnostics in the plasma with increasing N<sub>2</sub> gas flow rate. Thus, the particles in-flight velocity gradually increased with the N<sub>2</sub> gas flow, as explained during RPS of Al<sub>2</sub>O<sub>3</sub> powder (Ref 15). This increase in the particle velocity (with the N<sub>2</sub> gas flow) decreased its residence time in the plasma and thereby led to a worse melting behavior. Therefore, the transformation of  $\alpha$ -Al<sub>2</sub>O<sub>3</sub> to  $\gamma$ -phase decreased, and the coatings contain high  $\alpha$ -Al<sub>2</sub>O<sub>3</sub> content at higher N<sub>2</sub> flow rate. The particle velocity improved with the N<sub>2</sub> gas flow rate, and thus, the particles acceleration is attributed to the flow momentum and it strongly depends on the plasma gas mass flow rate. The nitrogen ions have higher mass flow rate than that of hydrogen (the ions of nitrogen are much heavier than hydrogen). Therefore, the particles acceleration is linked to nitrogen gas flow. It also reveals that such small increase in the arc current cannot compensate such high N<sub>2</sub> gas flow rate effect.

On the other hand, Fig. 11(b) shows the XRD spectrum of the heat-treated coating (arc current 650 A and N<sub>2</sub> gas of 160 SCFH) at 1100 °C for 12 h. The spectrum confirms the phase transformation of  $\gamma$ -Al<sub>2</sub>O<sub>3</sub> to  $\alpha$ -phase after heat treatment as was observed before in Fig. 10(d). Moreover, the transformation of the  $\gamma$ -Al<sub>2</sub>O<sub>3</sub> to  $\alpha$ -phase increased with increasing the heating time from 6 to 12 h. Herein, the arc current, N<sub>2</sub> gas flow and heat treatment affected the coating composition, and to optimize their effect, the coating microstructure was investigated. Figure 12 shows the cross-section microstructure of the coatings as function of arc current, N<sub>2</sub> gas flow rate, and post-treatment. The coating porosity increased with the arc current under low N<sub>2</sub> gas flow (Fig. 12b), and further increase was observed with the N<sub>2</sub> gas flow at 650 A

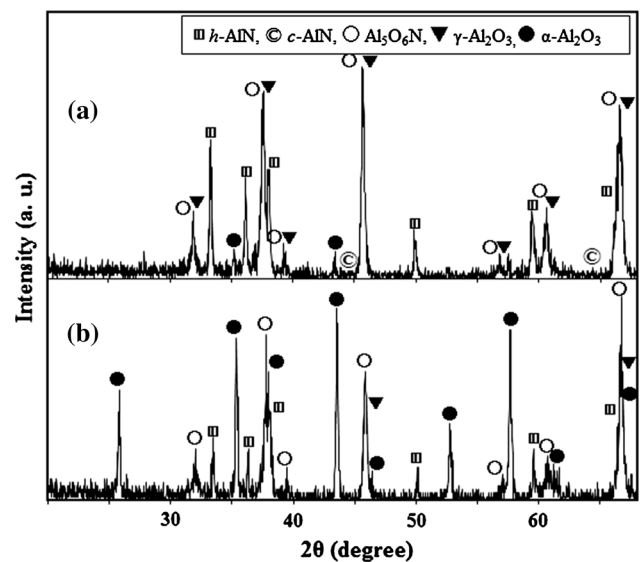


**Fig. 11** XRD spectra of the fabricated coating with using N<sub>2</sub> plasma gas flow rate of 160 SCFH and using A.C. of 650: (a) as sprayed (b) after heat treatment at 1100 °C for 12 h in N<sub>2</sub> gas ambient

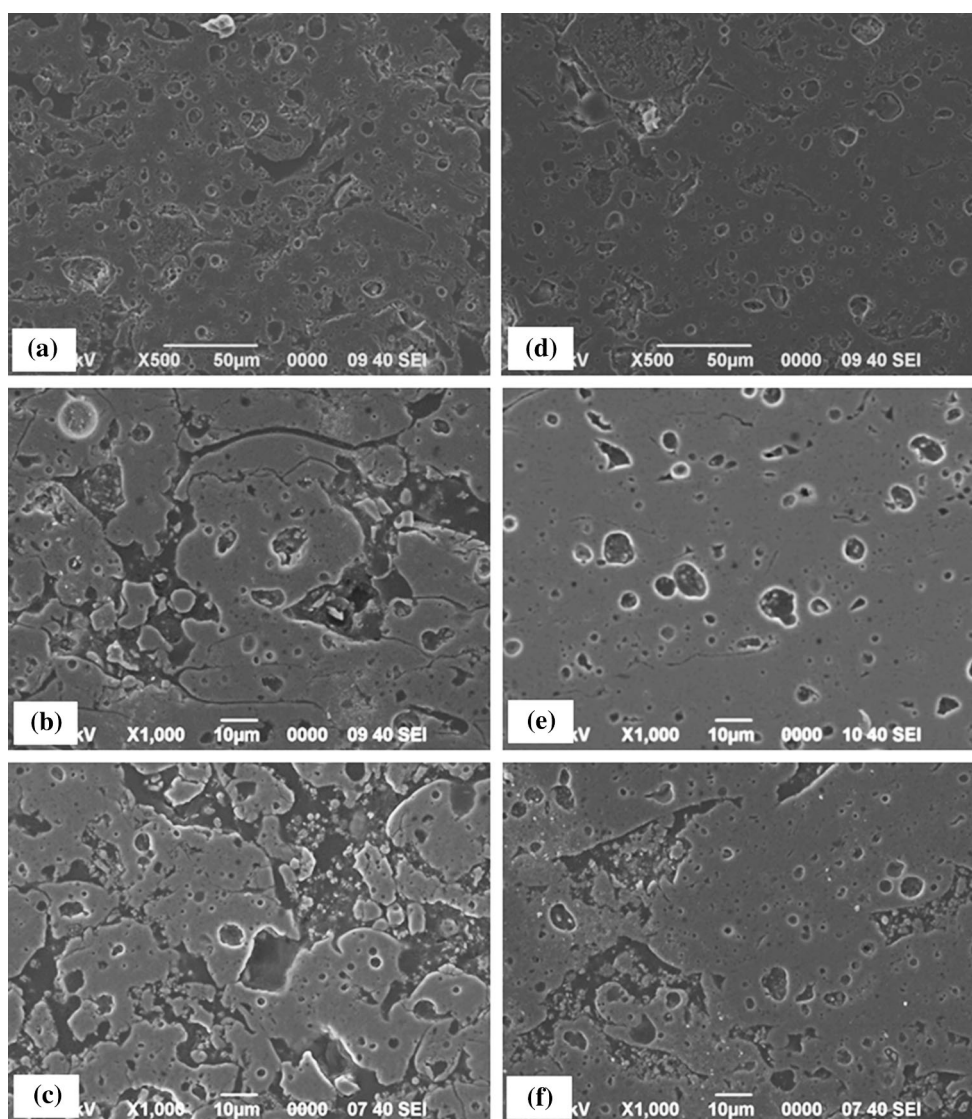
(Fig. 12c). On the other hand, after heat treatment, the splats had sintered together to some extent. This leads to decreasing the coating porosity after heat treatment especially at low  $N_2$  gas flow. Decreasing the coatings porosity after the heat treatment is well known in the field of thermal spray and may have an effect on the thermal conductivity.

Table 6 summarizes the thermal conductivity measurements values of the fabricated coatings as a function of  $N_2$  gas and arc current before and after heat treatment. It is clear that the coating thermal conductivity slightly improved with increasing the arc current. On the other hand, the effect of heat treatment is more significant than arc current and  $N_2$  gas flow. Furthermore, the heat treatment for the coating fabricated under low arc current and low  $N_2$  flow rate showed almost similar conductivity to the

coating fabricated under high arc current and higher  $N_2$  flow rate.

In order to understand and optimize the effect of each factor on the thermal conductivity, the coating porosity and phase content should be considered. Figure 13 shows the estimated values of the coatings porosity (estimated by image analysis of SEM cross section) and the relative amounts of the assigned phases (estimated by using Eq 10).

It is clear that each parameter (arc current,  $N_2$  gas flow) has some positive and negative effects with regard to the conductivity. For the as-sprayed coatings, increasing the arc current improves the  $h$ -AlN content (positive effect) and on the same time slightly increased the porosity,  $\gamma$ - $Al_2O_3$ , and  $Al_5O_6N$  (negative effects). Therefore, the increase in the thermal conductivity was not so big. Fur-



**Fig. 12** The SEM cross-section microstructure of the as-sprayed coatings at (a) 500 A— $N_2$  100 SCFH, (b) 650 A— $N_2$  100 SCFH, (c) 650 A— $N_2$  160 SCFH, and (d, e, and f) after heat treatment at 1100 °C for 12 h in  $N_2$  gas ambient, respectively

thermore, although increasing the N<sub>2</sub> gas under high arc current (N<sub>2</sub>: 160 and Arc: 650) improved the *h*-AlN content, decreased the  $\gamma$ -Al<sub>2</sub>O<sub>3</sub>, and Al<sub>5</sub>O<sub>6</sub>N (positive effects), it significantly increased the coating porosity (negative effect).

On the other hand, the post-heat treatment showed the most outstanding improvement in the conductivity. Generally, improving the thermal conductivity after heat treatment is well known in thermal spray field. It is mainly attributed to decreasing the coating porosity. Thus, the heat treatment has a tendency to reduce or eliminate the effect of splat-interface thermal resistance on the conductivity. However, the splats consist of small and slightly outstretched grains with some extensive distributed internal porosity, which give the low thermal conductivity for the coatings in total.

It is clear in Fig. 12 and 13 that, after heat treatment, the porosity,  $\gamma$ -Al<sub>2</sub>O<sub>3</sub>, and Al<sub>5</sub>O<sub>6</sub>N obviously decreased, and the  $\alpha$ -Al<sub>2</sub>O<sub>3</sub> phase significantly improved. The *h*-AlN

content was improved or remained the same after heat treatment. Therefore, the thermal conductivity was improved after heat treatment. Furthermore, the data showed that, after heat treatment at the same condition (1100 °C for 12 h), the conductivity of the coatings fabricated at low conditions (100 SCFH and 500 A) is almost same to the coatings fabricated at higher conditions (160 SCFH and 650 A). Thus, after the heat treatment, the 100 SCFH and 500 A coating showed lower porosity than the 160 SCFH and 650 A coating (although the AlN content was slightly lower). Therefore, using low N<sub>2</sub> gas flow and low arc current, followed by heat treatment is recommended. Moreover, the data showed that the heat treatment time may effect on the porosity and phase content of the coatings. However, its effect on the thermal conductivity was not so big basically under the current heat treatment conditions. Thus, with increasing the treatment time from 6 to 12 h, the decreasing tendency in the porosity,  $\gamma$ -Al<sub>2</sub>O<sub>3</sub>, and Al<sub>5</sub>O<sub>6</sub>N as well as the improve-

**Table 6** The thermal conductivity measurement values of the fabricated coatings at different spraying parameters of Ni gas flow and arc current before and after heat treatment

Spray parameters		Sample	Thickness, 10 <sup>-2</sup> m	$\rho$ , kg/m <sup>3</sup> (a)	$C_p$ , J/kg K(b)	$\alpha$ , ×10 <sup>-5</sup> m <sup>2</sup> /s(c)	$\lambda$ , W/m K(d)
N <sub>2</sub> , SCFH	Arc, A						
100	650	As spray	0.054	2540 ± 5	780 ± 1	1.58 ± 0.05	3.13
		1100 °C/6 h	0.042	2440 ± 5	788 ± 1	2.78 ± 0.05	5.35
100	500	As spray	0.051	2110 ± 5	770 ± 1	1.5 ± 0.05	2.44
		1100 °C/12 h	0.048	2280 ± 5	773 ± 1	3.24 ± 0.05	5.71
160	650	1100 °C/12 h	0.041	2230 ± 5	784 ± 1	3.27 ± 0.05	5.72

(a) The density measurement using Eq 7. (b) Two samples were measured (using Eq 6) and the average was considered. (c) THE diffusivity measurement using Eq 3. (d) The conductivity measurement using Eq 8  
± The uncertainty value for each measurement

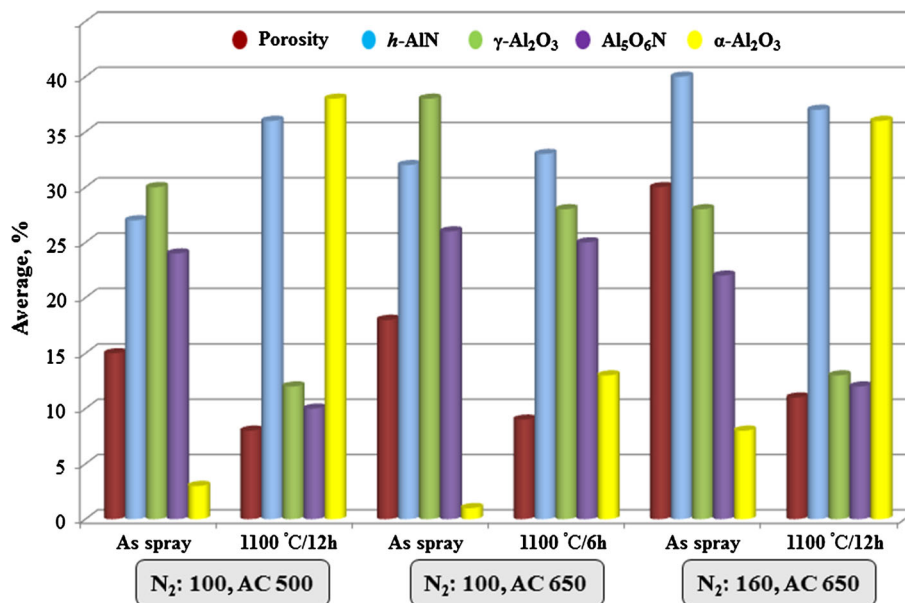
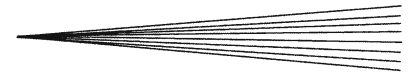


**Fig. 13** The estimated porosity and phase content of the fabricated coatings at different plasma-spraying parameters of N<sub>2</sub> gas flow and arc current before and after heat treatment (Color figure online)



ment in the conversion rate to the  $\alpha$ -Al<sub>2</sub>O<sub>3</sub> phase was observed, which is considered as a good indication for further studies.

Herein, the thermal conductivity of the reactive plasma-sprayed AlN coating was investigated as a function of N<sub>2</sub> gas, arc current, and heat treatment. The coatings thermal conductivity values are very low compared to the AlN compact conductivity. This is attributed to the coating phase composition, oxide content, and porosity level. The coating is a complicated system regarding the thermal conductivity. Optimizing the effect of each parameter is not that easy due to the variation of its effect on the coating phase composition, porosity, density, and therefore on its conductivity. Although the N<sub>2</sub> gas improved the AlN content, it obviously increased the porosity, and therefore, in total it had a negative effect on the thermal conductivity. In order to fabricate high thermal conductivity AlN plasma-sprayed coating, adjusting the oxide content and coating porosity at low N<sub>2</sub> gas flow rate and low arc current is recommended. One promising way to achieve high thermal conductivity AlN coating is the post-treatment of the fabricated coatings at low N<sub>2</sub> gas flow and low arc current, and it will be considered in further studies. Finally, it is worth mentioning that there are some more variables (besides the above-discussed variables) that must be considered particularly when dealing with the post-treatment, like the crystal size. Thus, the heat treatment will have a strong effect on the grain boundary and therefore on the heat transfer and thermal conductivity.

#### 4. Conclusion

The thermal conductivity of the aluminum nitride (AlN)/alumina (Al<sub>2</sub>O<sub>3</sub>) reactive plasma-sprayed coatings was investigated. The coating conductivity was very low compared to the AlN value. It is attributed to several factors in coatings: the phase composition, oxide content, density, and porosity. The presence of Al<sub>2</sub>O<sub>3</sub>, Al<sub>5</sub>O<sub>6</sub>N and high coating porosity decreased the thermal conductivity. The following results were obtained in this study:

- The oxygen in the AlN lattice creates aluminum vacancies which lead to phonon scattering and therefore decrease the AlN thermal conductivity. The low density and high porosity of coatings suppressed the thermal conductivity.
- Although the N<sub>2</sub> gas flow rate improved the nitriding conversion, it suppressed the thermal conductivity gradually, due to the further increase in the coating porosity and further decrease of its density with the N<sub>2</sub> gas.
- The arc current did not have a significant effect on the AlN coating thermal conductivity. Thus, it increased the porosity as well as the AlN content. Optimizing the influence of each parameter separately on the thermal conductivity is quite difficult for such coating composition. This is due to the variation of each parameter ef-

fect on the phase composition, porosity, density, and therefore on the conductivity.

- The most significant factor is the heat treatment. Thus, it improved the coating thermal conductivity under all conditions. Thus, after heat treatment, the porosity,  $\gamma$ -Al<sub>2</sub>O<sub>3</sub>, and Al<sub>5</sub>O<sub>6</sub>N obviously decreased, and the  $\alpha$ -Al<sub>2</sub>O<sub>3</sub> phase significantly improved. Increasing the N<sub>2</sub> gas and the arc current did not show any significant effect on the conductivity after heat treatment.
- In order to fabricate high thermal conductivity AlN coatings, adjusting the oxide content, coating porosity, and microstructure through the post-heat treatment at low N<sub>2</sub> gas flow rate and low arc current is recommended.

#### Acknowledgments

This research was supported by the Grants-in-Aid for JSPS Fellows (232575) of Japan Society for the Promotion of Science (JSPS).

#### References

1. G. Selvaduray and L. Sheet, Aluminum Nitride: Review of Synthesis Methods, *Mater. Sci. Technol.*, 1993, **9**, p 463-473
2. H.O. Pierson, *Handbook of Refractory Carbides and Nitrides*, Noyes, Hammon, 1996, p 237-239
3. A.W. Wemer, *Carbide, Nitride and Boride Materials Synthesis and Processing*, Chapman & Hall, London, 1997, p 6-68
4. E.I. Meletis and S. Yan, Formation of Aluminum Nitride by Intensified Plasma Ion Nitriding, *J. Vac. Sci. Technol. A*, 1991, **9**(4), p 2279-2284
5. W.D. Kingery, H.K. Bowen, and D.R. Uhlmann, *Introduction to Ceramic*, Wiley, New York, 1976, p 583
6. J.-E. Sundgren, Structure and Properties of TiN Coatings, *Thin Solid Films*, 1985, **128**, p 21-44
7. P. Fauchais, A. Vardelle, and B. Dussoubs, Quo Vadis Thermal Spraying?, *J. Therm. Spray Technol.*, 2001, **10**(1), p 44-66
8. M.F.O. Schiefler Filho, A.J.A. Buschinelli, F. Gärtner, A. Kirsten, J. Voyer, and H. Kreye, Influence of Process Parameters on the Quality of Thermally Sprayed X46Cr13 Stainless Steel Coatings, *J. Braz. Soc. Mech. Sci. Eng.*, 2004, **26**(1), p 98-106
9. M. Shahien, M. Yamada, T. Yasui, and M. Fukumoto, *In Situ* Fabrication of AlN Coating by Reactive Plasma Spraying of Al/AlN Powder, *Coatings*, 2011, **1-2**, p 88-107
10. M. Shahien, M. Yamada, T. Yasui, and M. Fukumoto, Reactive Atmospheric Plasma Spraying of AlN Coatings: Influence of Aluminum Feedstock Particle Size, *J. Therm. Spray Technol.*, 2011, **20**(3), p 580-589
11. M. Shahien, M. Yamada, T. Yasui, and M. Fukumoto, Influence of NH<sub>4</sub>Cl Powder Addition for Fabrication of Aluminum Nitride Coating in Reactive Atmospheric Plasma Spray Process, *J. Therm. Spray Technol.*, 2011, **20**(1-2), p 205-212
12. M. Shahien, M. Yamada, T. Yasui, and M. Fukumoto, Influence of Plasma Gases on Fabrication of AlN Coatings Through Atmospheric Plasma Nitriding Process, *Ind. Appl. Plasma Process.*, 2010, **3**, p 1-10
13. M. Shahien, M. Yamada, T. Yasui, and M. Fukumoto, Cubic Aluminum Nitride Coating Through Atmospheric Reactive Plasma Nitriding, *J. Therm. Spray Technol.*, 2010, **19**(3), p 635-641
14. M. Shahien, M. Yamada, T. Yasui, and M. Fukumoto, Fabrication of AlN Coatings by Reactive Atmospheric Plasma Spray Nitriding of Al Powders, *Mater. Trans.*, 2010, **51**(5), p 957-961

15. M. Shahien, M. Yamada, T. Yasui, and M. Fukumoto, N<sub>2</sub> and H<sub>2</sub> Plasma Gases' Effects in Reactive Plasma Spraying of Al<sub>2</sub>O<sub>3</sub> Powder, *Surf. Coat. Technol.*, 2013, **216**, p 308-317
16. M. Shahien, M. Yamada, T. Yasui, and M. Fukumoto, Synthesis of Cubic Aluminum Nitride Coating from Al<sub>2</sub>O<sub>3</sub> Powder in Reactive Plasma Spray process, *Mater. Trans.*, 2013, **54**(2), p 207-214
17. M. Shahien, M. Yamada, T. Yasui, and M. Fukumoto, Fabrication of AlN/Al<sub>2</sub>O<sub>3</sub> Coatings via Atmospheric Reactive Plasma Nitriding of Al<sub>2</sub>O<sub>3</sub> Powders, *Key Eng. Mater.*, 2011, **484**, p 166-171
18. M. Shahien, M. Yamada, T. Yasui, and M. Fukumoto, Reactive Plasma Spraying of Fine Al<sub>2</sub>O<sub>3</sub>/AlN Feedstock Powder, *J. Therm. Spray Technol.*, 2013, **22**(8), p 1283-1293
19. W.J. Parker, R.J. Jenkins, C.P. Butler, and G.L. Abbott, A Flash Method of Determining Thermal Diffusivity, Heat Capacity, and Thermal Conductivity, *J. Appl. Phys.*, 1961, **32**, p 1679-1684
20. JIS R1611, *Measurement Methods of Thermal Diffusivity, Specific Heat Capacity, and Thermal Conductivity for Fine Ceramics by Flash Method*, Japan Industrial Standards, Tokyo, 2010
21. ISO 18755, *Fine Ceramics (Advanced Ceramics, Advanced Technical Ceramics)—Determination of Thermal Diffusivity of Monolithic Ceramics by Laser Flash Method*, International Organization for Standardization, Geneva, 2005
22. M.J. O'Neill, Measurement of Specific Heat Functions by Differential Scanning Calorimetry, *Anal. Chem.*, 1966, **38**(10), p 1331-1336
23. JIS R1672, *Determination of Specific Heat of Fiber-Reinforced Ceramics Composite by Differential Scanning Calorimetry Methods*, Japan Industrial Standards, Tokyo, 2006
24. JIS K 7123, *Testing Methods for Specific Heat Capacity of Plastics*, Japan Industrial Standards, Tokyo, 1987
25. F.Y.C. Boey, X.L. Song, Z.Y. Gu, and A. Tok, AlN Phase Formation in a Tape-Cast Al<sub>2</sub>O<sub>3</sub>/AlN Composite, *J. Mater. Process. Technol.*, 1999, **89**(90), p 478-480
26. G.A. Slack, Nonmetallic Crystals with High Thermal Conductivity, *J. Phys. Chem. Solids*, 1973, **34**(2), p 321-335
27. G.A. Slack, R.A. Tanzilli, R.O. Pohl, and J.W. Vandersande, The Intrinsic Thermal-Conductivity of AlN, *J. Phys. Chem. Solids*, 1987, **48**(7), p 641-647
28. A.V. Virkar, T.B. Jackson, and R.A. Cutler, Thermodynamic and Kinetic Effects of Oxygen Removal on the Thermal Conductivity of Aluminum Nitride, *J. Am. Ceram. Soc.*, 1989, **72**(11), p 2031-2042
29. N.N. Ault, Characteristics of Refractory Oxide Coatings Produced by Flame-Spraying, *J. Am. Ceram. Soc.*, 1957, **40**, p 69-74
30. G.F. Hurley and F.D. Gac, Structure and Thermal Diffusivity of Plasma-Sprayed Al<sub>2</sub>O<sub>3</sub>, *Am. Ceram. Soc. Bull.*, 1979, **58**(5), p 509-511
31. K.S. Ravichandran, K. An, R.E. Dutton, and S.L. Semiatin, Thermal Conductivity of Plasma-Sprayed Monolithic and Multilayer Coatings of Alumina and Yttria-Stabilized Zirconia, *J. Am. Ceram. Soc.*, 1999, **82**(3), p 673-682
32. S. Boire-Lavigne, C. Moreau, and R.G. Saintjacques, The Relationship Between the Microstructure and Thermal Diffusivity of Plasma-Sprayed Tungsten Coatings, *J. Therm. Spray Technol.*, 1995, **4**(3), p 261-267
33. S. Raghavan, H. Wang, R.B. Dinwiddie, W.D. Porter, and M. Mayo, Effect of Grain Size, Porosity and Yttria Content on the Thermal Conductivity of Nanocrystalline Zirconia, *Scr. Mater.*, 1998, **39**(8), p 1119-1125
34. L.H. Cao, K.A. Khor, L. Fu, and F. Boey, Plasma Spray Processing of Al<sub>2</sub>O<sub>3</sub>/AlN Composite Powders, *J. Mater. Process. Technol.*, 1999, **89**(90), p 392-398
35. R.J. Damani and P. Makroczy, Heat Treatment Induced Phase and Microstructural Development in Bulk Plasma Sprayed Alumina, *J. Eur. Ceram. Soc.*, 2000, **20**(7), p 867-888